The Evolution of El Niño-Precipitation Relationships from Satellites and Gauges

By

Scott Curtis
Joint Center for Earth Systems Technology
Department of Geography and Environmental Systems
University of Maryland, Baltimore County
NASA / Goddard Space Flight Center
Greenbelt, MD 20771

And

Robert F. Adler
NASA / Goddard Space Flight Center
Greenbelt, MD 20771

Submitted to Journal of Climate April 16,2002

Abstract

This study uses a twenty-three year (1979-2001) satellite-gauge merged community data set to further describe the relationship between El Niño Southern Oscillation (ENSO) and precipitation. The globally complete precipitation fields reveal coherent bands of anomalies that extend from the tropics to the polar regions. Also, ENSO-precipitation relationships were analyzed during the six strongest El Niños from 1979 to 2001. Seasons of evolution, Pre-onset, Onset, Peak, Decay, and Post-decay, were identified based on the strength of the El Niño. Then two simple and independent models, first order harmonic and linear, were fit to the monthly time series of normalized precipitation anomalies for each grid block. The sinusoidal model represents a three-phase evolution of precipitation, either dry-wet-dry or wet-dry-wet. This model is also highly correlated with the evolution of sea surface temperatures in the equatorial Pacific. The linear model represents a two-phase evolution of precipitation, either dry-wet or wet-dry. These models combine to account for over 50% of the precipitation variability for over half the globe during El Niño. Most regions, especially away from the Equator, favor the linear model. Areas that show the largest trend from dry to wet are southeastern Australia, eastern Indian Ocean, southern Japan, and off the coast of Peru. The northern tropical Pacific and Southeast Asia show the opposite trend.

1. Introduction

Ever since the definition of the Southern Oscillation (SO) (Walker and Bliss 1932) there have been earnest attempts to link interannual climate variations in the tropics with global precipitation anomalies (e.g. Rasmusson and Carpenter 1983, Kousky et al. 1984, Aceituno 1988, and Kiladis and Diaz 1989). Ropelewski and Halpert (1986, 1987) defined typical global and regional precipitation anomaly patterns during El Niño/Southern Oscillation (ENSO) episodes from 1877 to 1976. This work was expanded to include changes in the distribution of precipitation during ENSO (Ropelewski and Halpert 1996). Furthermore, Mason and Goddard (2001) extended the Ropelewski and Halpert (1987) analysis by using a high-resolution gridded data set over land for 1951 to 1996.

However, for a truly global perspective on precipitation variations accompanying ENSO, one must rely on climate models (Smith and Ropelewski 1997) or use satellite observations of precipitation. Satellite-gauge merged precipitation products have the advantage of being observationally-based, globally complete, and tied to surface measurements. Although the period of satellite coverage (1979 to present) is relatively short compared to the majority of gauge records, it is a period of strong and frequent ENSO events and thus useful for developing relationships between ENSO and global precipitation patterns.

Huffman et al. (1997), in the release of the Global Precipitation Climatology Project (GPCP) Version 1 data set, offered difference maps between the 1991/92 El Niño and 1988/89 La Niña. Xie and Arkin (1997) showed difference maps between warm and cold ENSO episodes. Trenberth and Caron (2000) updated global ENSO-precipitation correlation patterns and Dai and Wigley (2000) used EOFs of satellite information combined with century-long rain gauge records to characterize ENSO-induced precipitation variability. These analyses inherently assume a linear relationship between precipitation anomalies and the phases of ENSO (wet/dry during La Niña; dry/wet during El Niño). Also, while seasonal depictions of ENSO are given, these analyses are ultimately snapshots of ENSO and little is said of the evolution of precipitation anomalies during a typical warm or cold event. Here we characterize El Niños from 1981 to 2000 with the most recently developed merged satellite-gauge rainfall product - GPCP Version 2 (Adler et al. 2002). Regions are identified that experience significant precipitation anomalies in either two or three stages during a typical El Niño.

2. Data

GPCP is the World Climate Research Program (WCRP) / Global Energy and Water Cycle Experiment (GEWEX) project devoted to producing community analyses of global precipitation. GPCP's Version 2 monthly data set (hereafter referred to as GPCP)

is an extension of Huffman et al. (1997) in space and time. Aside form low-orbit–satellite microwave, geosynchronous-orbit–satellite infrared, and rain gauge inputs described in Huffman et al. (1997), GPCP includes TOVS data (Susskind et al. 1997) to fill in missing or uncertain data in high latitudes and OPI data (Xie and Arkin 1998) trained on the 1987-1998 period to extend back in time. The end product is a monthly globally complete observational precipitation data set at a 2.5 degree grid from 1979 to present.

A recent application of GPCP was monthly indices of ENSO in terms of precipitation anomalies associated with the Walker Circulation (Curtis and Adler 2000). In summary, area averages of precipitation anomalies were calculated throughout larger domains encompassing the Maritime Continent and central Pacific. The largest positive anomaly in the Pacific was subtracted by the largest negative anomaly in the Maritime Continent, and the normalized difference was defined as the El Niño Index (EI). Likewise, the largest positive anomaly in the Maritime Continent was subtracted by the largest negative anomaly in the Pacific, and the normalized difference was defined as the La Niña Index (LI). Finally, the two indices were combined into the ENSO Precipitation Index (ESPI), where positive values indicate the warm phase of ENSO and negative values the cold phase. A weakened Walker Circulation (positive ESPI) during El Niño induces large shifts in tropical convection, which through anomalous latent heat release, changes large-scale flow regimes, and ultimately affects global precipitation patterns.

3. Global El Niño-precipitation relationships

Fig. 1 shows normalized precipitation anomalies for El Niño and La Niña composites based on ESPI and the El Niño minus La Niña difference. As discussed in previous studies (see section 1), when precipitation is enhanced over the central Pacific and reduced over the Maritime Continent, during El Niño, then rain rates are anomalously high off the horn of Africa, central Asia, the southern Indian Ocean, the southeast Pacific, the Gulf coast of the U.S., and North Atlantic (Fig. 1a). Rain rates are anomalously low throughout much of Africa, the southwest Pacific, the Caribbean, the Amazon basin and equatorial Atlantic, and the southern tip of South America (Fig. 1a). Whereas, during La Niña, when precipitation is enhanced over the Maritime Continent and reduced over the Pacific, precipitation anomalies are of opposite sign to those described above (Fig. 1b). This is reflected by the fact that the difference field (Fig. 1c) is very similar to the El Niño map (Fig. 1a). Roughly two thirds of the globe is either, wet during La Niña and dry during El Niño, or dry during La Niña and wet during El Niño. This suggests that the remaining third of the Earth either has a nonlinear relationship with ENSO or is unrelated to ENSO. For example, North Africa, the eastern subtropical North Pacific, and the Northeast U.S. are dry for both La Niña and El Niño. In the Southern Hemisphere New Zealand is dry for El Niño and La Niña, whereas just to the south it is wet during both phases of ENSO.

While there are obvious ENSO-precipitation relationships in the tropics, interesting features are also seen in the mid- to high latitudes. The El Niño minus La Niña difference (Fig. 1c) produces precipitation departures with spatial continuity over large distances. The canonical precipitation anomalies over land appear to be connected via the oceans in a horseshoe pattern. Wet conditions extend in the Southern hemisphere from the Pacific southeastward across Chile and Argentina into the South Atlantic Ocean. In the Northern hemisphere the counterpart feature extends across the southern U.S. and Atlantic Ocean into Europe (Fig. 1c). Further to the west a negative anomaly extends southeastward from the Maritime Continent across the South Pacific and through the Drake Passage. The Norhtern hemisphere counterpart crosses the North Pacific and southern Canada (Fig. 1c). Finally, enhanced precipitation extends from the horn of Africa northward to central Asia. The southern counterpart appears to extend as far south as the Ross Sea (Fig. 1c). These patterns are also seen in polar projections of the Northern and Southern hemispheres, Fig. 2a and b respectively. Negative precipitation anomalies are found in the western North Pacific and Canada while positive precipitation anomalies dominate Asia and extend in a band from the tropics through the U.S. and into the North Atlantic (Fig. 2a). This banded structure is even more apparent in the Southern Hemisphere (Fig. 2b), where there are fewer land masses to impede precipitation signals emanating from the tropics. Positive precipitation anomalies from the central Pacific and Indian Oceans and negative anomalies from Australia spiral into the Antarctica continent.

This is consistent with a study by Sinclair et al. (1997) which showed a similar pattern in ECMWF mean sea level pressure and cyclone density anomalies during El Niño.

4. Evolution of global precipitation anomalies

The typical El Niño evolution is here defined as the average of the six episodes, from 1981 to 2001. We purposefully exclude the questionable 1979-80 El Niño, which is weak according to standard El Niño definitions (Trenberth 1997) and not accompanied by any signal in the ESPI. Fig. 3 shows the 24-month evolution of ESPI used to define the 1982-83, 1986-87, 1991-92, 1992-93, 1994-95, and 1997-98 El Niños. Pre-onset is defined as the three or four months before the ESPI goes positive. Onset, Peak, and Decay months, all with positive ESPI values, are grouped somewhat subjectively. Onset (Decay) months lead (follow) the Peak months and have generally lower ESPI values (Table 1). Post-decay months are defined as the three or four months that follow after ESPI goes negative.

Each El Niño event differs in overall strength, position within the annual cycle and length (Table 1). For example the 1982-83 event peaks between October and February, while the 1986-87 event peaks between March and August. The 1991-92 event has a very long Onset stage, while the 1992-93 event has a very long Decay stage. Thus, the results from this section are meant to show average conditions and are not necessarily applicable to individual events. A more detailed description of rainfall patterns during

each of the six episodes is given in the Appendix. Furthermore, the characterization of an individual El Niño can be somewhat dependant on the metric used. Table 1 shows that the SST in the Nino3.4 region was highest during the 1982-83 episode, while the gradient of anomalous precipitation measured by ESPI was most pronounced during 1997-98. Also, for five out of the six El Niños the peak ESPI value led the peak Nino3.4 value by 1 to 5 months (Table 1).

4.a Composite maps

First the months used to define the six El Niño episodes were sorted based on their ESPI values and divided equally into five sets. Global percentile-ranked precipitation anomalies were then averaged over each set. The top three quintiles account for over 75% of the months used to create Fig. 1a. Precipitation patterns associated with the strongest El Niño months (Fig. 4a) are very similar to those shown in Fig. 1a, however the precipitation anomalies are somewhat weaker and the global horseshoe patterns are more disjointed, especially in the southern hemisphere. Anomalies in the second (Fig. 4b) and third (Fig. 4c) quintiles, serve to fill in these discontinuities. For example, an area of enhanced rainfall in the Indian Ocean in the second quintile (Fig. 4b) falls between two centers of positive precipitation anomalies in the first quintile, off the horn of Africa and to the east of Madagascar (Fig. 4a). Negative anomalies to the east of the Drake Passage in the third quintile (Fig. 4c) extend the deficit of precipitation found to the west of the Drake Passage in both first (Fig. 4a) and second quintiles (Fig. 4b).

The fourth (Fig. 4d) and fifth (Fig. 4e) quintiles are mostly composed of pre-onset and post-decay months and do not contribute to the global El Niño-precipitation relationships.

Next, the normalized precipitation anomalies are shown for the Pre-onset, Onset, Peak, Decay, and Post-decay stages, defined in Fig. 3. Pre-onset (Fig. 5a) resembles a weak La Niña event. The most striking feature is negative precipitation anomalies covering the southern tropical Pacific contrasting with positive anomalies to the north including Hawaii. The Onset composite (Fig. 5b) shows a weakening Walker circulation, with positive precipitation anomalies appearing first in the central Pacific, just north of the Equator, and negative anomalies blanketing the Maritime Continent. Drier than normal conditions are also found in the Caribbean Sea, consistent with previous studies (Hastenrath 1976, 1984; Giannini et al. 2000). Interestingly, a southwest-northeast oriented line connects these three centers of action. The spatial continuity of anomalies, mentioned in section 3, is already present during Onset. Reduced rainfall stretches from the Maritime Continent southeastward to a band in the southern oceans and northeastward to the U.S. West Coast. Enhanced rainfall in the central Pacific extends southeastward across southern South America and northeastward through the southern U.S.

The Peak composite (Fig. 5c) is similar to Fig. 1a. The major anomaly centers are aligned zonally along the Equator, but branch out into the mid-latitudes. During this stage the positive anomaly horseshoe emerges in the western Indian Ocean. The Decay

composite (Fig. 5d) shows a weakening of the global connectivity. The zonal gradient of precipitation anomalies, used to construct the ESPI, is weaker than the meridional gradients in the central Pacific. The negative anomalies over the Maritime Continent have dissipated, while the center of enhanced rainfall has moved south of the Equator, sandwiched between bands of below normal rainfall. It is dry over Mexico and northeast Brazil and wet in the South Atlantic Convergence Zone. The Post-decay composite (Fig. 5e) has La Niña characteristics, but does not particularly resemble the Pre-Onset composite (Fig. 5a).

A few areas of the globe are dominated by positive or negative precipitation anomalies throughout El Niño from Onset to Decay. However, many regions are both wet and dry during the course of the evolution. For example, in the U.S. during Onset the west is dry and southeast wet, while during Decay the anomalies are of the opposite sign (Fig. 5a,c). On average Australia, southern Japan, eastern Indian Ocean, and the seas south of New Zealand begin dry and end wet. These intra-El Niño variations in precipitation are of particular interest and raise the question: can the evolution from the onset months to the decay months be empirically modeled so as to provide a framework for regional predictions based on ENSO?

4.b Simple models

Ropelewski and Halpert (1987) provide a benchmark in describing the global evolution of El Niño-related precipitation, using a first order harmonic (FOH) fit to

twenty-four months of data. Their analysis can produce a two-phase evolution of precipitation (dry-wet or wet-dry) if the beginning and ending points are near zero, a three-phase evolution (dry-wet-dry or wet-dry-wet) if the beginning and ending points are close to either the maximum or minimum, or a combination of the two. For example, the evolution of sea surface temperature in the central Pacific occurs in three phases (Fig. 6a).

Here we take a different approach and attempt to separate two possible precipitation responses to El Niño with two empirical models of evolution. First, a thirteen-month time range is used to depict the El Niño evolution. This is chosen so as to exclude most of the Pre-onset and Post-decay months, which are influenced by La Niña (Fig. 4), and accommodate the short 1994-95 event. Fig. 6a shows Nino3.4 SST anomalies for the six-El Niño average (Fig. 3). Precipitation in the central Pacific should follow a similar evolution. The three-phase model is simply a normalized first order harmonic with the maximum centered on zero (Fig. 6b). The two-phase model represents the linear component of precipitation evolution (Fig. 6b).

Next the variance explained by both models was computed at all grid blocks for the three-month running mean of normalized precipitation anomalies during the thirteen-month El Niño episode. The two models account for more than half of the variance for 51% of the globe (Fig. 7a). The variance explained exceeds 0.9 in two bands on either side of the equator in the Pacific. Other areas where the precipitation evolution is

essentially a combination of the two models include southern Mexico, northern South America, the Maritime Continent, and South Africa. Examining the models separately (Figs. 7b,c) reveals that for most of the world, more of the total variance during El Niño is attributed to the linear rather than the sinusoidal model. Precipitation shows the expected three-phase evolution over the Nino3.4 domain (Fig. 7b). The sinusoidal model also characterizes well precipitation over Mexico, the Pacific Northwest states, Alaska, the southern Indian Ocean, and South Africa. In order to determine the sign of the relationship, a regression map was plotted (Fig. 8a). Mexico, the Northwest states, and southern Indian Ocean are dry during the Onset stage of El Niño, then become wet with the mature El Niño before becoming dry again during the Decay stage. The opposite occurs in Alaska and South Africa (Fig. 8a). The linear or two-phase model shows high power over Northwest Canada, much of the tropical Pacific outside of the equatorial strip, the eastern Indian Ocean, and southeast Australia (Fig. 7c). Fig. 8b reveals that the north tropical Pacific dries during the course of El Niño, while the east-central Pacific, just south of the Equator, gets wetter. This was seen during the 1997-98 El Niño (Curtis et al. 2001). Northwest Canada goes from wet to dry and the eastern Indian Ocean and southeastern Australia go from dry to wet.

Finally, by examining Fig. 8a and b together, movements of precipitation anomaly centers from Onset to Decay can be identified. One example occurs over the western U.S. and Canada. The Northwest U.S. extending out into the Pacific shows a significant

three-phase evolution (Fig. 8a), with a wet anomaly during the Peak phase (Fig. 5c). Both to the north and to the south a two-phase evolution dominates (Fig. 8b) with western Canada experiencing a wet Onset and dry Decay, and the opposite occurring over California (Fig. 5b,d). This suggests a southward migration of the positive precipitation anomaly center during the lifecycle of the El Niño and may represent a southward shift in the preferred North Pacific storm track from Onset to Decay.

5. Discussion

This study is a further attempt to quantify ENSO-precipitation relationships on a global scale, with regional applications. GPCP has the unique advantage of being both globally complete and based on observations from space borne instruments and surface gauges. The record is now over twenty years long and contains the two largest El Niño events of the 20th century. Thus, with only 6 events, a strong El Niño signal emerges in the analysis.

It was shown that ENSO affects precipitation from the tropics to the high-latitudes via eastward directed bands that spiral into the polar regions. This pattern is somewhat incomplete when examining only the strongest El Niño months, as the weaker El Niño months account for part of the observed connectivity.

On average, about two thirds of the Earth's precipitation had a linear relationship to the phases of ENSO from 1979 to 2000. However, the remaining one third of the

globe had precipitation anomalies of the same sign regardless of the phase of ENSO. The nonlinearities in the ENSO-precipitation relationship increase as one tries to characterize the typical evolution. Thus, this study focused on the 1982-83, 1986-87, 1991-92, 1992-93, 1994-95, and 1997-98 El Niños. A similar study regarding La Niña events from 1979 to 2000 is underway.

Pre-onset, Onset, Peak, Decay, and Post-Decay composites were constructed from the six events. On average positive precipitation anomalies appear in the central Pacific first and move eastward and then southward as the event matures. The largest negative anomalies are found over the Maritime Continent and South Pacific during Onset, but shift to the central Pacific during the Decay stage.

Most of the world shows both wet and dry anomalies during the El Niño life cycle. Here we quantified regional precipitation changes based on two models - a sinusoidal three-phase evolution and a linear two-phase evolution. A combination of these models describes the typical El Niño response for the majority of the globe. The three-phase evolution model is particularly strong over the central Pacific where precipitation is tied to the evolution of SST. The two-phase evolution model depicts the shift of convection from the western to eastern equatorial Pacific and the drying of the north tropical Pacific during El Niños. Many of the traditional ENSO-precipitation relationships over land (Mexico and Gulf, Amazonia, South Africa) show a three-phase evolution of precipitation. Oceanic and high-latitude regions favor a two-phase

evolution. Another two-phase evolution occurs in southeast Australia, which is dry during onset and wet during decay.

Unlike many previous studies, here we removed the annual cycle and showed the global evolution of precipitation based on the normalized strength of the zonal gradient of precipitation anomalies in the Pacific. Many regions were identified that experienced changes in precipitation in two and three stages during a thirteen-month El Niño cycle. In that regard, this study provides a framework for ENSO-based precipitation predictions.

Appendix

Here the Onset, Peak, and Decay phases of the individual El Niño episodes are described in chronological order. In section (a) the 1982-83, (b) the 1986-87, (c) the 1991-92, (d) the 1992-93, (e) the 1994-95, and (f) the 1997-98 El Niños are described. A summary is given in section (g).

a. 1982-83

It can be argued that the 1982-83 El Niño was stronger than any other event in the twentieth century (Table 1). During the Onset phase regions of the Maritime Continent are below the twentieth percentile, while a band of above average rainfall stretches from the western U.S. to the west tropical Pacific (Fig. 9a). Pan-America is drier than normal and central South America and eastern Africa are wet. During the Peak there is a strong weakening of the Walker Circulation as much of the Maritime Continent and eastern

Australia are extremely dry and the rain rates exceed the ninetieth percentile for much of the equatorial Pacific (Fig. 9b). Northeast Brazil is dry and the East African horseshoe, described in section 3, is well developed. In the Decay phase the precipitation anomalies have a zonal orientation in the northern hemisphere, with negative values in the tropics and positive values in the mid-latitudes (Fig. 9c). Enhanced rainfall is found in the Pacific off the coast of South America and in the Atlantic around 30° N and S. The Atlantic Intertropical Convergence Zone appears drier than normal.

b. 1986-87

Above average precipitation is observed in the equatorial Pacific, at the date line, during the Onset phase of the 1986-87 El Niño (Fig. 9d). However, the Maritime Continent is not dry, but rather the north Pacific is, around 30°. At the Peak, the positive anomaly shows only a slight intensification and movement eastward (Fig. 9e). Negative anomalies now appear from the Maritime Continent to the south Pacific. Precipitation anomalies are generally weak and not well organized during the Decay phase (Fig. 9f). It should be noted that central Africa is wet, which is unusual for this phase of El Niño.

c. 1991-92

The 1990s were a period of frequent warm episodes, beginning with the 1991-92 El Niño. Extreme events are muted in the average of the long Onset phase (Fig. 3c). A third of the months that make up the Onset composite (Fig. 5b) are taken from this event. Thus, it is not surprising to see negative anomalies over the Maritime Continent, positive

anomalies in the equatorial Pacific and negative anomalies in the Caribbean (Fig. 10a). During the short Peak phase, anomalies near the tenth percentile extend from the western Pacific, through southeast Asia and India, and into much of the African continent (Fig. 10b). Highlights of the Decay stage include a deficit of rain over the equatorial Atlantic and Eastern Europe (Fig. 10c).

d. 1992-93

The 1991-92 El Niño was immediately followed by another warming of the equatorial Pacific during 1993. The Onset phase appears to be a combination of El Niño and La Niña precipitation patterns (Fig. 1a,b). Negative anomalies cover the eastern equatorial Pacific and Maritime Continent, while positive anomalies stretch from the western Pacific northeastward to North America and southeastward to the coast of Chile (Fig. 10d). An arch of enhanced rainfall is anchored on the horn of Africa. These global connections are absent during the Peak phase (Fig. 10e). This phase is characterized by a local gradient of anomalous precipitation between New Guinea/northern Australia and the western equatorial Pacific. An area of extremely dry conditions is located just to the north of the center of enhanced rainfall. The Inter Americas Sea and northwest U.S. are wet. The gradient identified in the Peak phase continues into the Decay phase (Fig. 10f). The northwest Indian Ocean is one area with abundant rainfall.

e. 1994-95

The 1994-95 warming was accompanied by a slight weakening of the Walker Circulation, as observed from precipitation. The Australian continent was extremely dry during the Onset phase (Fig. 11a). A strong Indian Ocean dipole dominates the Peak phase (Fig. 11b). The two-month Decay phase is noisy and the extremes are likely unrelated to El Niño (Fig. 11c).

f. 1997-98

The 1997-98 El Niño is in sharp contrast to the 1994-95 episode. A coherent gradient of precipitation anomalies between the Maritime Continent and western Pacific is seen during Onset (Fig. 11d). The gradient expands to encompass the entire equatorial Pacific and eastern Indian Ocean during the Peak phase (Fig. 11e). This strong gradient is reflected by the largest ESPI values on record (Table 1). Strong negative anomalies cover Amazonia, northeast Canada, and central Africa. Negative anomalies extend from the Maritime Continent southeastward to Antarctica. During the Decay phase the rainfall deficit over the Maritime Continent ends. However, strong negative anomalies extend from the Philippines to the west coast of Mexico (Fig. 11f). Strong positive anomalies are found over the U.S. west coast, eastern China, and western Indian Ocean.

g. Summary

The maps presented here can serve as a reference for global precipitation anomalies during El Niños since 1981. However, it must be understood that global

extremes are highly dependent on the number of months that comprise each phase. It should also be noted that the 1982-83 fields (Fig. 9a,b,c) and the 1986-87 onset (Fig. 9d) are much smoother than the other maps. This is an effect of the inhomogeneity of the GPCP data set. OPI, which is the only input data set over ocean prior to 1986, is constructed from a linear regression relationship with OLR anomalies. Microwave estimates of precipitation, which begin in July 1987, are physically related to hydrometeors. The difference between detecting cold clouds and cold cloud precipitation gives rise to the difference in spatial variability.

As expected the strong 1982-83 and 1997-98 El Niños are most similar. These are the only two events where precipitation anomalies over the ninetieth percentile reach the coast of South America. Also, these are the only events where the Decay phase is characterized by a strong meridional gradient of precipitation anomalies in the North Pacific. Differences are most apparent, when examining the global response during the six El Niño events. Strong anomalies from a couple of El Niños often overcome weaker anomalies of the opposite sign from the remaining events. Sometimes this is indicative of longer-term variability. For example in India rainfall rates were reduced during the peaks of the 1982-83, 1986-87, and 1991-92 El Niños, but normal during the peaks of the 1992-93, 1994-95, and 1997-98 events. Also, a region may have a consistent response to El Niño but occurring in different stages of evolution. For example, during the 1982-83 El Niño Mexico was dry during Onset and wet during the Peak, but during the 1997-98

El Niño Mexico was wet during Onset and dry during the Peak. Despite the normalization process, a seasonal effect may still be present, especially in regions with pronounced annual cycles like Mexico.

Table 1. Measures of the evolution, longevity, and strength of the six El Niños since 1981.

El Niño	1982-83	1986-87	1991-92	1992-93	1994-95	1997-98
Length	14	15	16	14	9	16
# Onset Months	4	4	10	4	3	5
# Peak Months	5	6	3	3	4	5
# Decay Months	5	5	3	7	2	6
ESPI avg. Onset	1.19	0.67	0.81	0.32	0.37	1.13
Nino3.4 avg. Onset	1.24	1.29	0.99	0.18	0.35	0.44
ESPI avg. Peak	1.91	1.31	1.65	0.76	0.99	2.28
Nino3.4 avg. Peak	2.47	1.43	1.70	0.83	0.82	2.34
ESPI avg. Decay	0.79	0.47	0.64	0.33	0.63	1.35
Nino3.4 avg. Decay	0.99	1.33	0.73	0.39	1.22	1.78
Max ESPI (month)	2.39 (Nov. 82)	1.65 (Apr. 87)	2.09 (Mar. 92)	1.38 (Apr. 93)	1.32 (Sep. 94)	2.94 (Jun. 97)
Max Nino3.4 (month)	2.85 (Jan. 83)	1.88 (Aug. 87)	1.94 (Feb. 92)	1.06 (May 93)	1.40 (Dec. 94)	2.80 (Nov. 97)

Figure Captions

Fig. 1 Composites of normalized precipitation for El Niño and La Niña from 1979 to September 2001 based on the ENSO Precipitation Index (ESPI). (a) El Niño: the 91 months with the highest ESPI values, (b) La Niña: the 91 months with the lowest ESPI values, and (c) El Niño minus La Niña. Color bar indicates the number of standard deviations away from the mean. Multiply values by two for El Niño minus La Niña

Fig. 2 Same as Figure 1a, except in gray-scale and restricted to a) the Northern hemisphere and b) the Southern hemisphere.

Fig. 3 Evolution of six El Niño events based on the 3-month running mean of ESPI. (-) indicates months considered pre-onset, (O) onset months, (P) peak months, (D) decay months, and (+) post-decay months. A) Bold line represents the 1982-83 El Niño. B) Bold line represents the 1986-87 El Niño. C) Bold line represents the 1991-92 El Niño. D) Bold line represents the 1992-93 El Niño. E) Bold line represents the 1994-95 El Niño. F) Bold line represents the 1997-98 El Niño.

Fig. 4 Composites of normalized precipitation anomalies based on the magnitude of ESPI. Months identified in Figure 3 were ranked according to their ESPI value and divided into five equal sets. A) First twenty-three months, B) second twenty-three months, C) third twenty-three months, D) fourth twenty-three months, E) fifth twenty-three months.

Fig. 5 Composite evolution of normalized precipitation anomalies during the six identified El Niño events. See Fig. 3 for definitions of the 5 stages. A) Pre-Onset, B) Onset, C) Peak, D) Decay, and E) Post-decay. Color bar indicates the ranked percentage, where 50 is normal.

Fig. 6 A) Time series of 3-month running mean of Nino3.4 averaged for the six El Niño events and centered on the peak month. B) Normalized (-1 to 1) first harmonic, solid line, and linear, dashed line, models of the precipitation response to El Niño.

Fig. 7 Variance of the normalized precipitation anomalies explained by the models given in Fig. 5b. A) Variance explained (0.4 to 1.0) by a regression of both the sinusoidal and linear values. B) Variance explained (0.4 to 1.0) by the sinusoidal model alone.
C) Variance explained (0.4 to 10.0) by the linear model alone.

Fig. 8 Colors indicate the regression coefficients for A) the first harmonic model and B) the linear model onto the normalized precipitation anomalies. Contours indicate significance at the 5% level based on the null hypothesis that the regression coefficients are zero.

Fig. 9 Normalized precipitation anomalies for the 1982-83 and 1986-87 El Niños. A) 1982-83 Onset, B) 1982-83 Peak, C) 1982-83 Decay, D) 1986-87 Onset, E) 1986-87 Peak, F) 1986-87 Decay. See Figure 3 for specific months used.

Fig. 10 Normalized precipitation anomalies for the 1991-92 and 1992-93 El Niños. A) 1991-92 Onset, B) 1991-92 Peak, C) 1991-92 Decay, D) 1992-93 Onset, E) 1992-93 Peak, F) 1992-93 Decay. See Figure 3 for specific months used.

Fig. 11 Normalized precipitation anomalies for the 1994-95 and 1997-98 El Niños. A) 1994-95 Onset, B) 1994-95 Peak, C) 1994-95 Decay, D) 1997-98 Onset, E) 1997-98 Peak, F) 1997-98 Decay. See Figure 3 for specific months used.

Fig. 1

a) El Nino

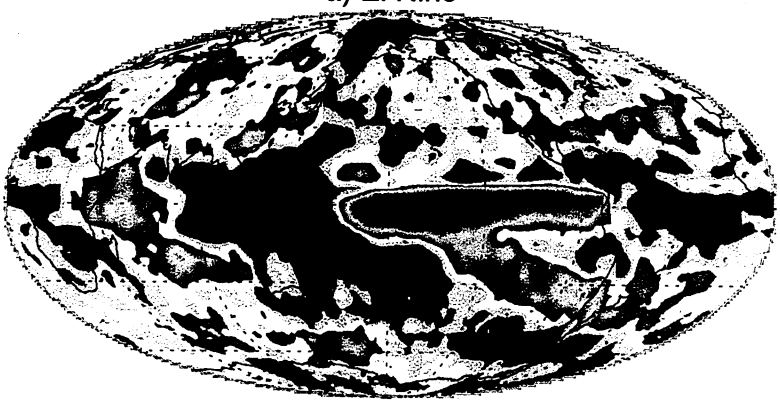

b) La Nina

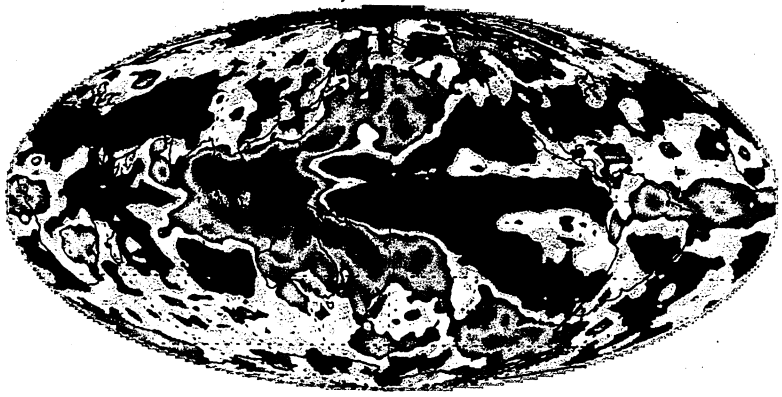

c) El Nino - La Nina

-0.6 -0.3 0.0 0.3 0.6

(x2) for El Nino - La Nina

Fig 2

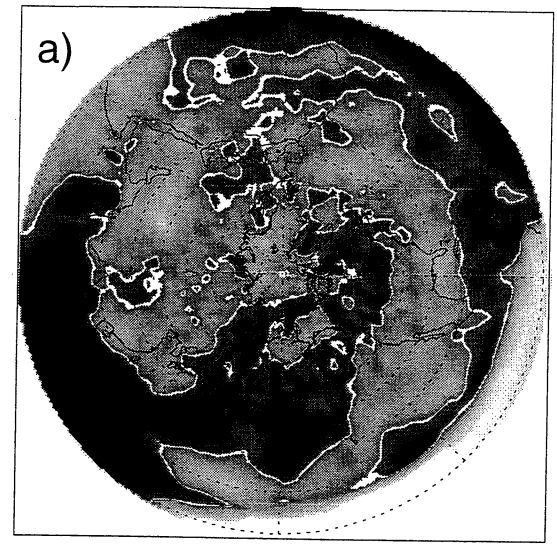

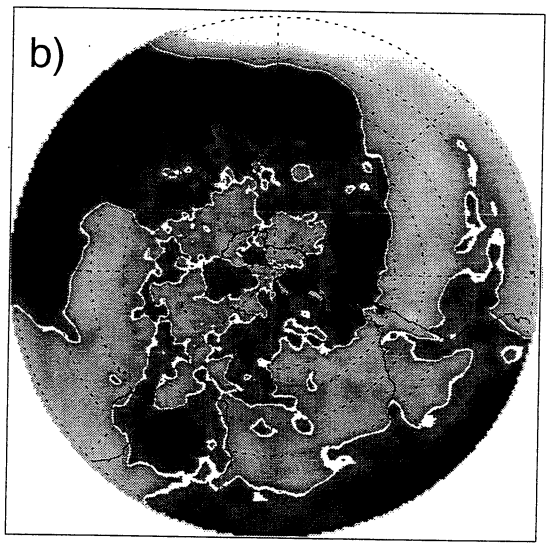

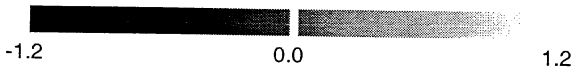

Fig 3

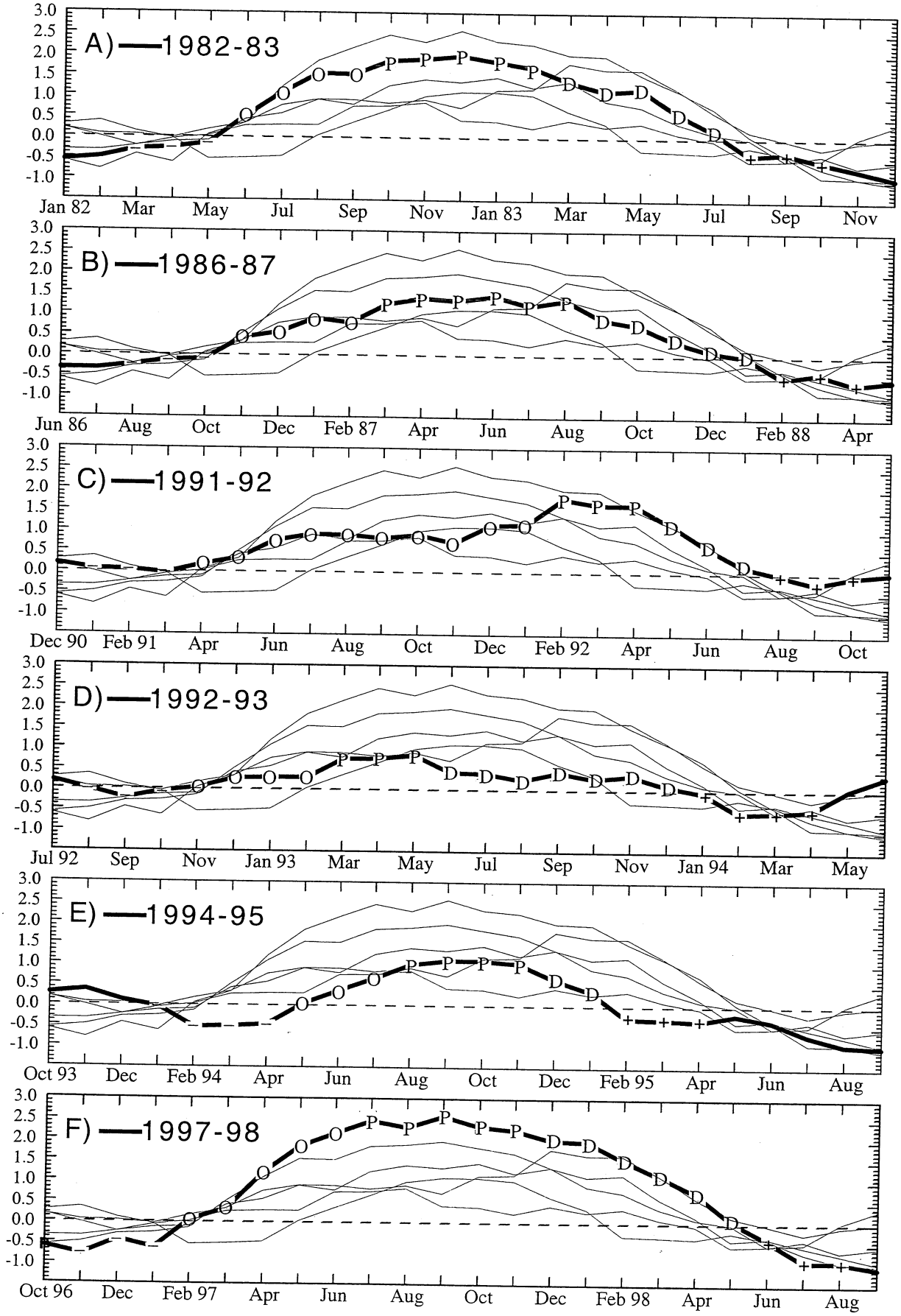
A) —1982-83
3.0
2.5
2.0
1.5
1.0
0.5
0.0
-0.5
-1.0
Jan 82
Mar
May
Jul
Sep
Nov
Jan 83
Mar
May
Jul
Sep
Nov
B) —1986-87
Jun 86
Aug
Oct
Dec
Feb 87
Apr
Jun
Aug
Oct
Dec
Feb 88
Apr
C) —1991-92
Dec 90
Feb 91
Apr
Jun
Aug
Oct
Dec
Feb 92
Apr
Jun
Aug
Oct
D) —1992-93
Jul 92
Sep
Nov
Jan 93
Mar
May
Jul
Sep
Nov
Jan 94
Mar
May
E) —1994-95
Oct 93
Dec
Feb 94
Apr
Jun
Aug
Oct
Dec
Feb 95
Apr
Jun
Aug
F) —1997-98
Oct 96
Dec
Feb 97
Apr
Jun
Aug
Oct
Dec
Feb 98
Apr
Jun
Aug

Fig 4

a) First ESPI Composite

b) Second ESPI Composite

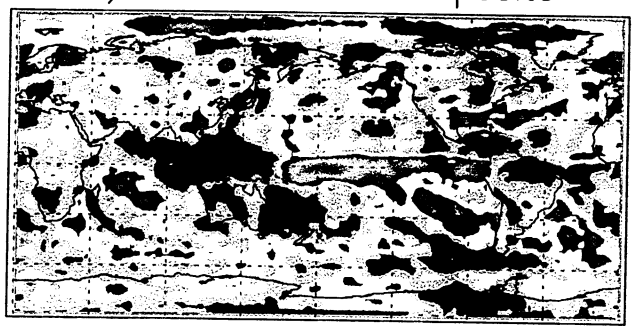

c) Third ESPI Composite

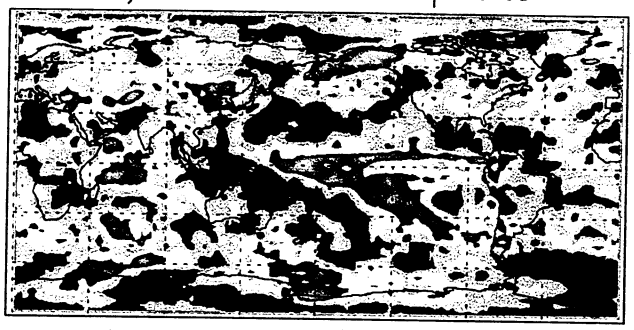

d) Fourth ESPI Composite

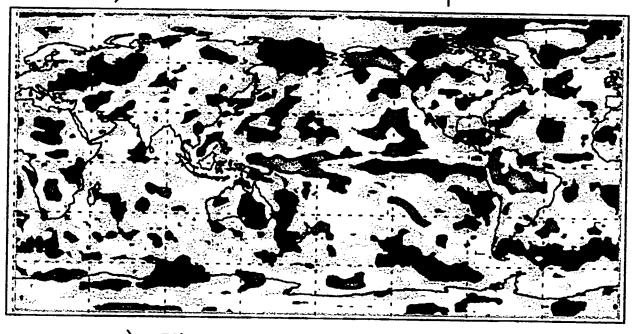

e) Fifth ESPI Composite

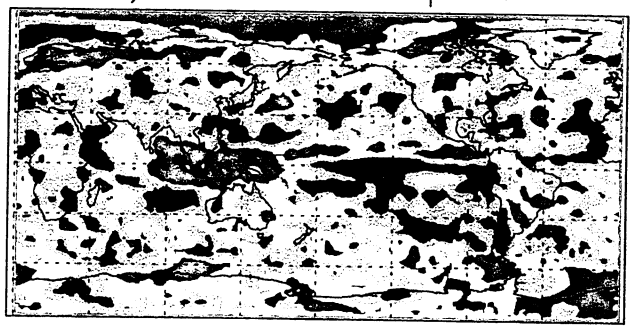

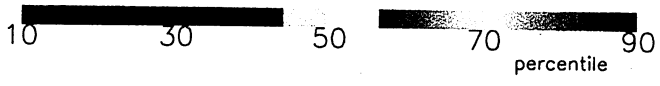

Fig 5

a) Pre–Onset Composite

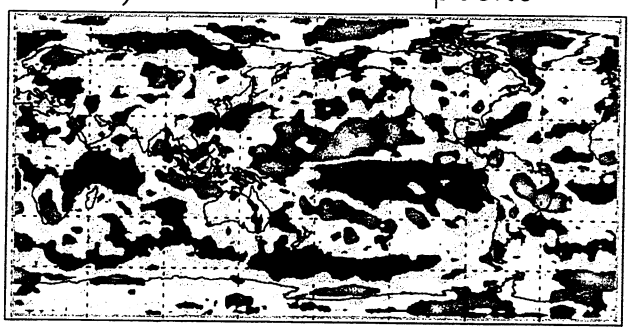

b) Onset Composite

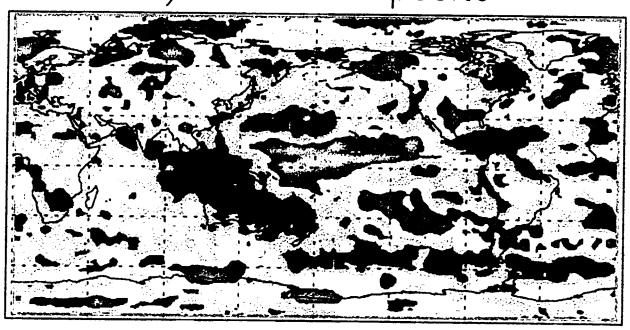

c) Peak Composite

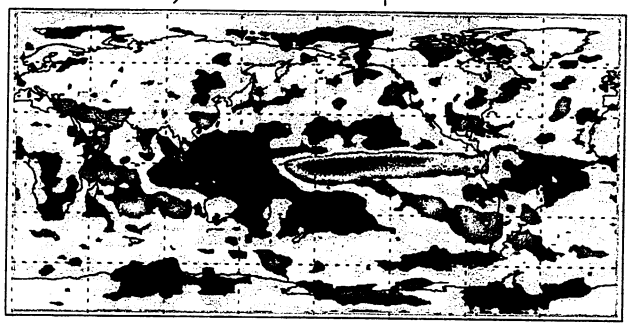

d) Decay Composite

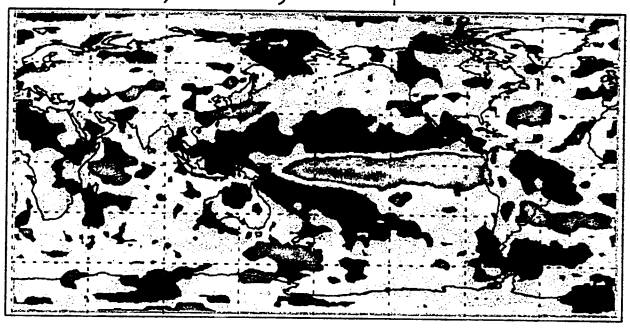

e) Post–Decay Composite

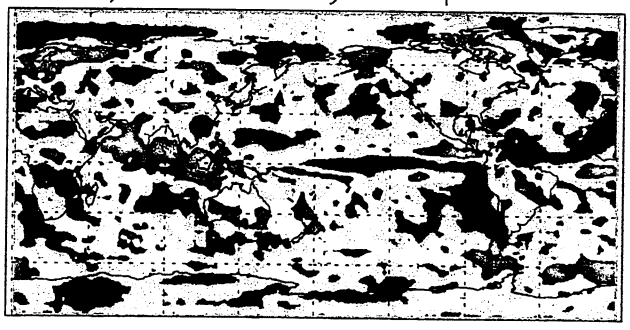

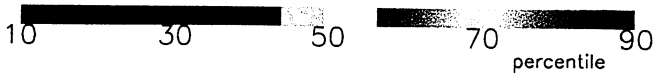

Fig. 6

A) Nino3.4 Evolution Over Six Events

3–month running mean; time series centered on peak month

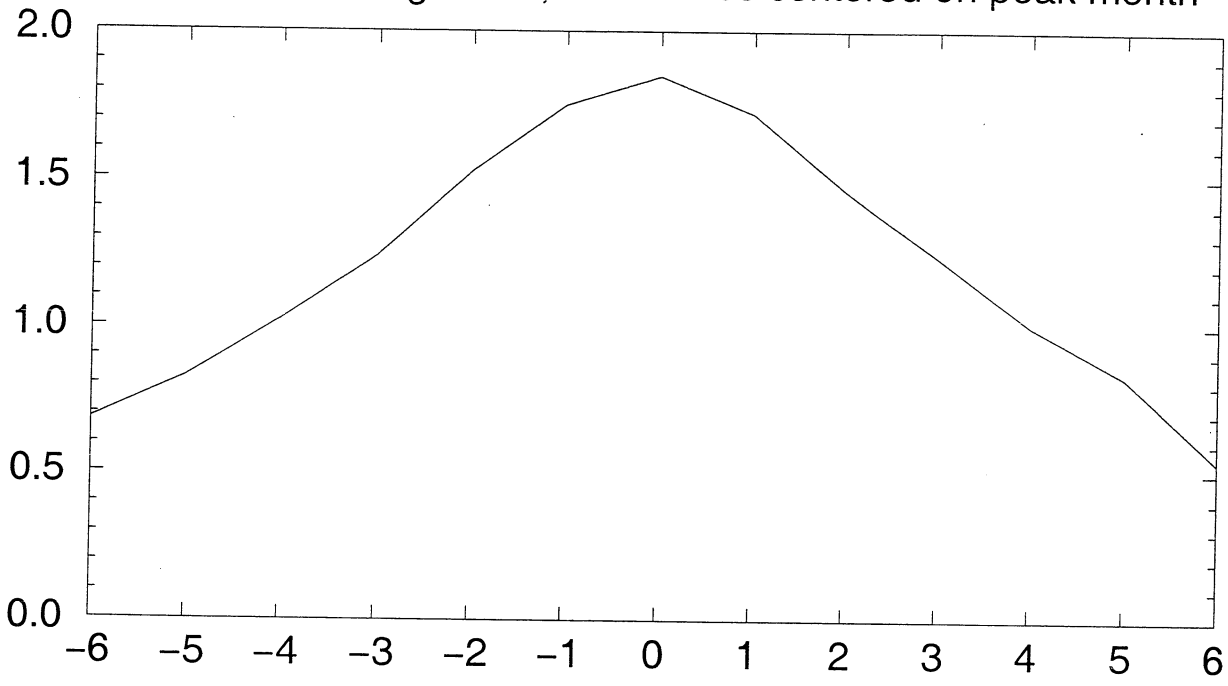

B) Sinusoidal and Linear Models

of Precipitation Response to El Nino

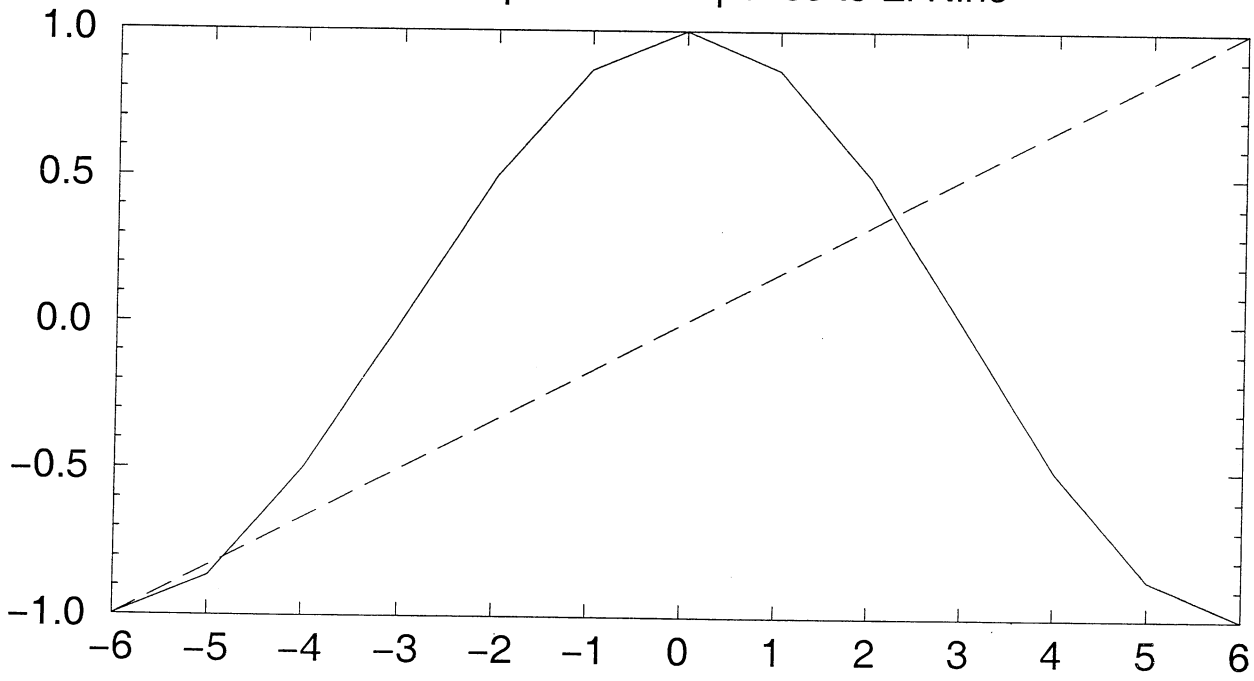

Fig. 7

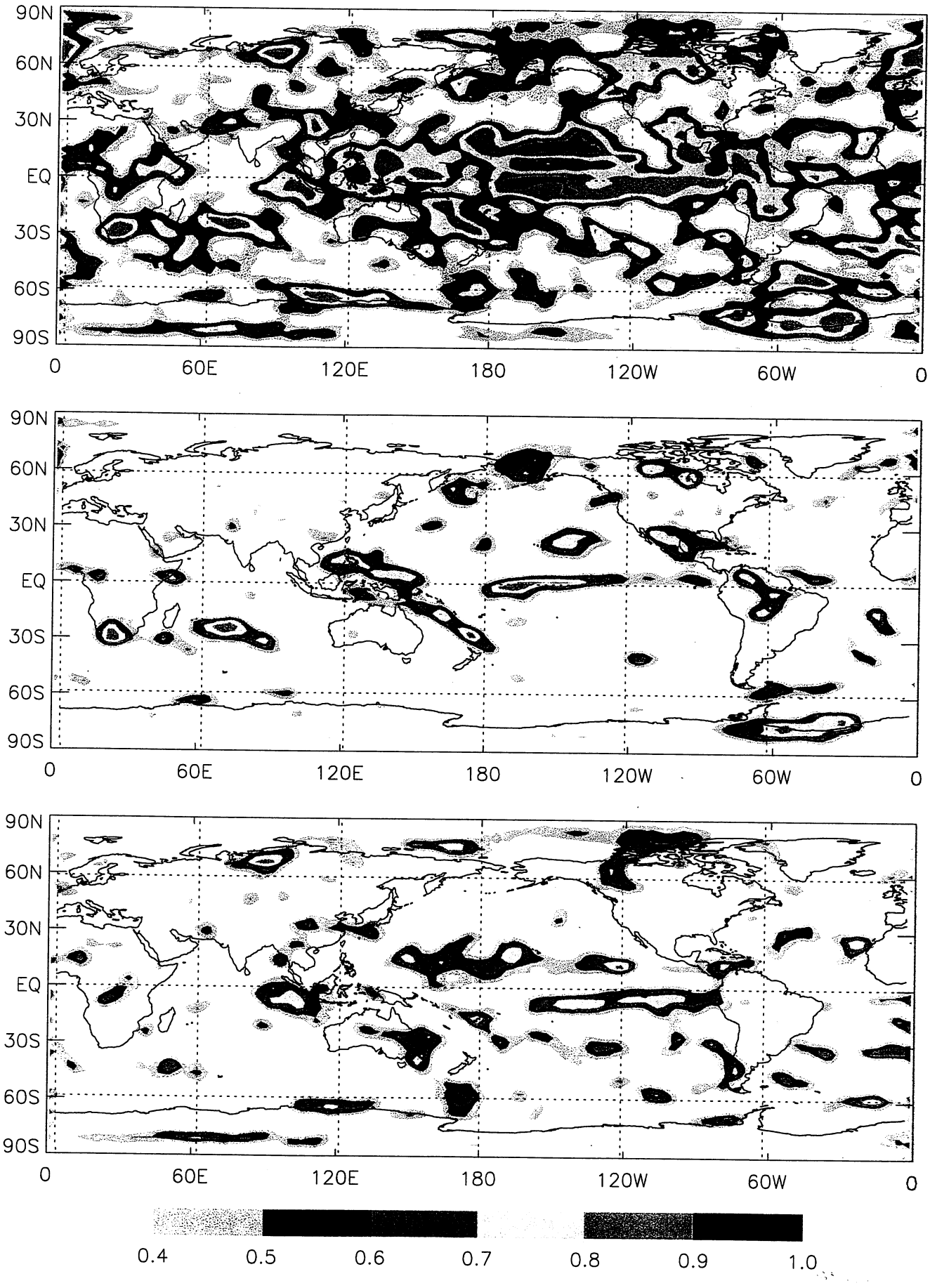
90N
60N
30N
EQ
30S
60S
90S
0
60E
120E
180
120W
60W
0
0.4
0.5
0.6
0.7
0.8
0.9
1.0

Fig. 8

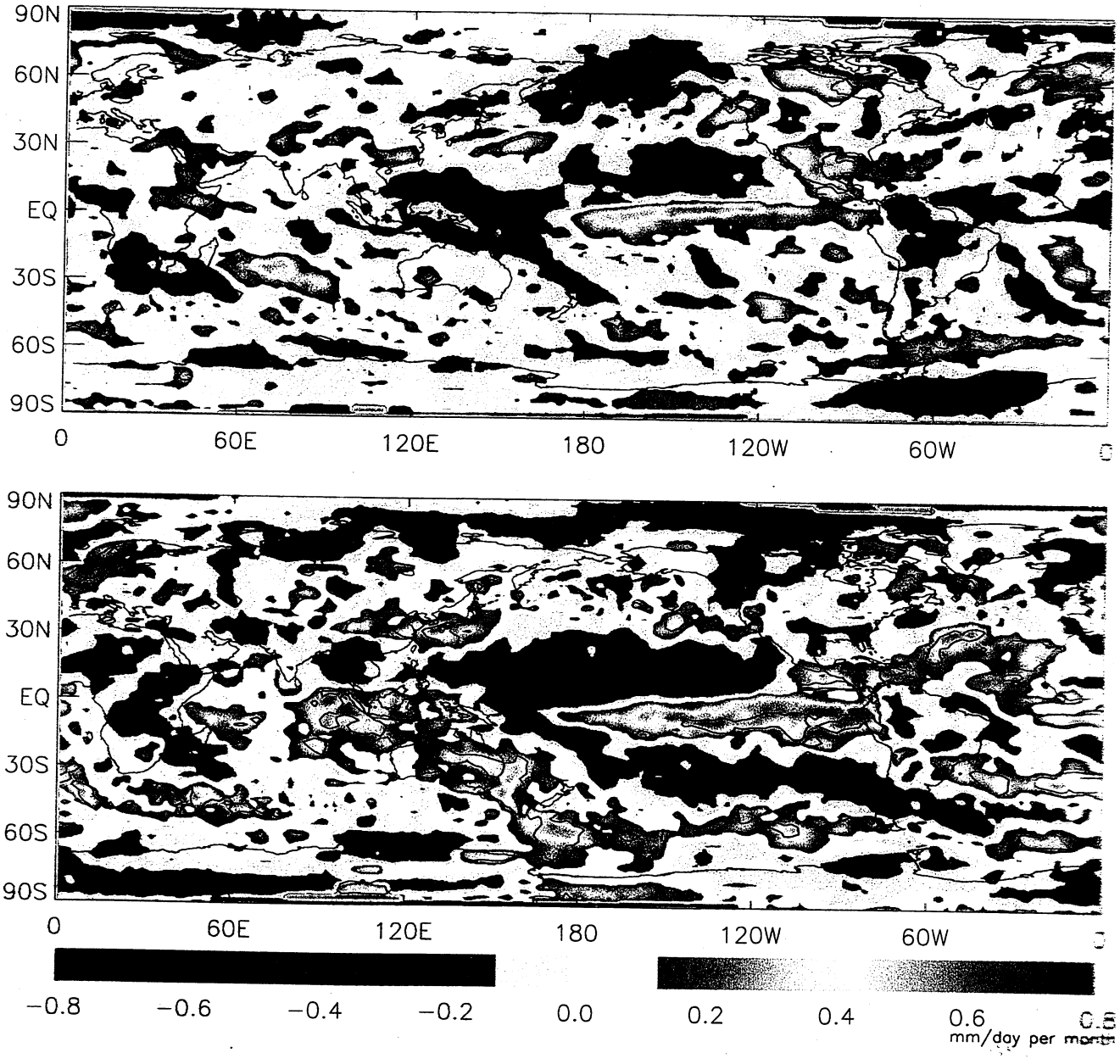
90N
60N
30N
EQ
30S
60S
90S
0
60E
120E
180
120W
60W
−0.8
−0.6
−0.4
−0.2
0.0
0.2
0.4
0.6
mm/day per month

Fig. 9

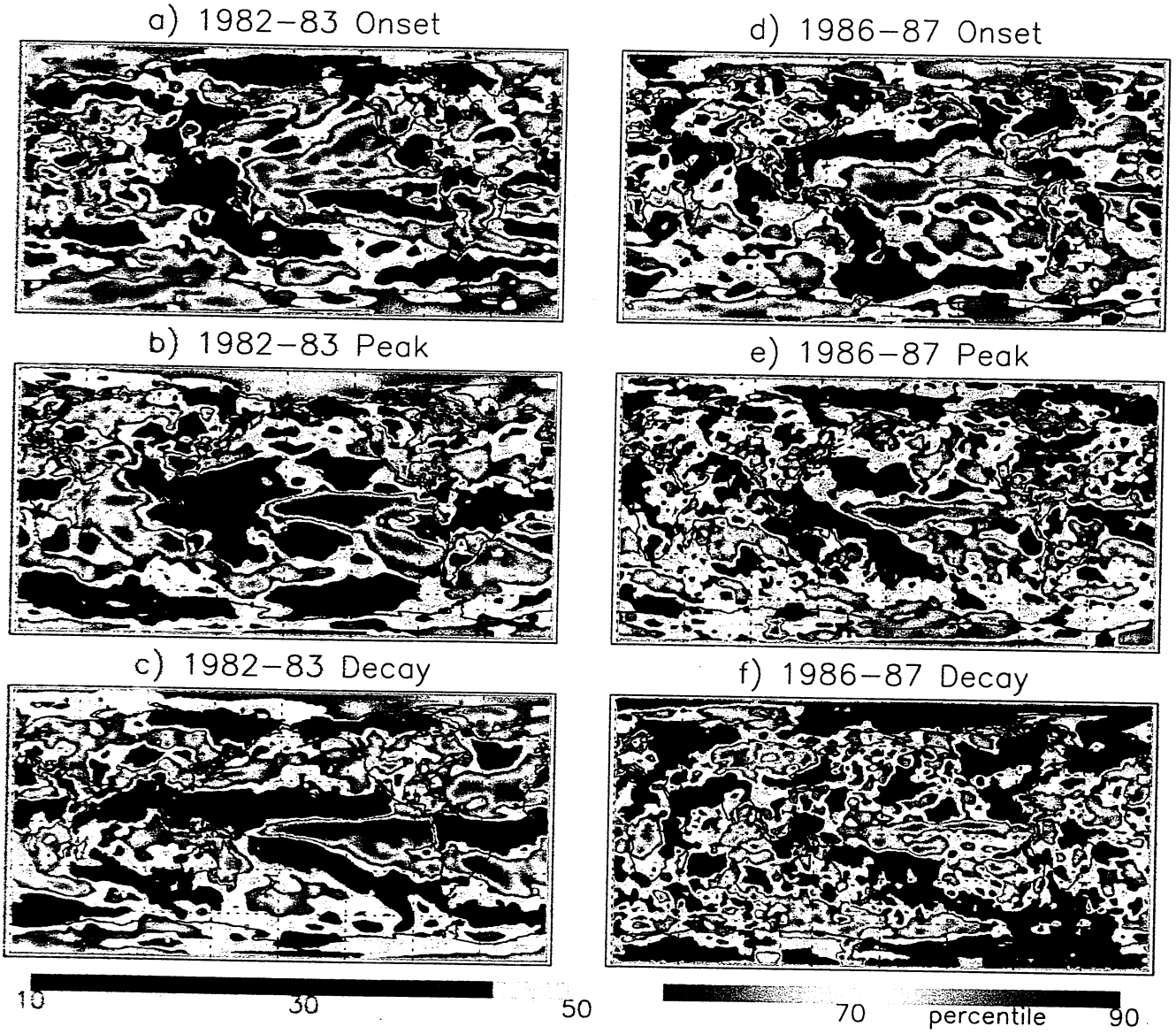
a) 1982–83 Onset
d) 1986–87 Onset
b) 1982–83 Peak
e) 1986–87 Peak
c) 1982–83 Decay
f) 1986–87 Decay
10
30
50
70
percentile
90

Fig. 10

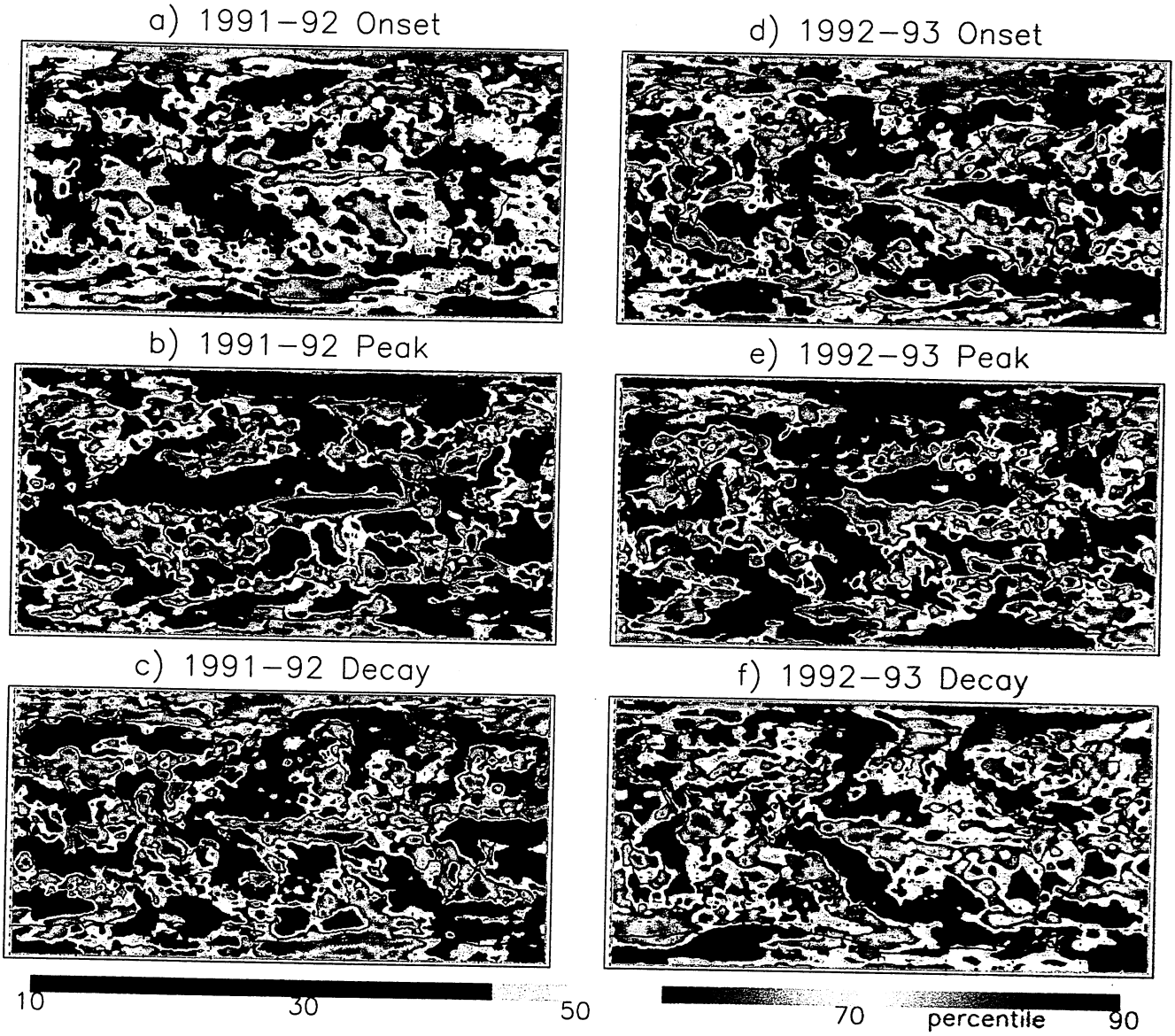
a) 1991–92 Onset
d) 1992–93 Onset
b) 1991–92 Peak
e) 1992–93 Peak
c) 1991–92 Decay
f) 1992–93 Decay
10
30
50
70
percentile
90

Fig. 11

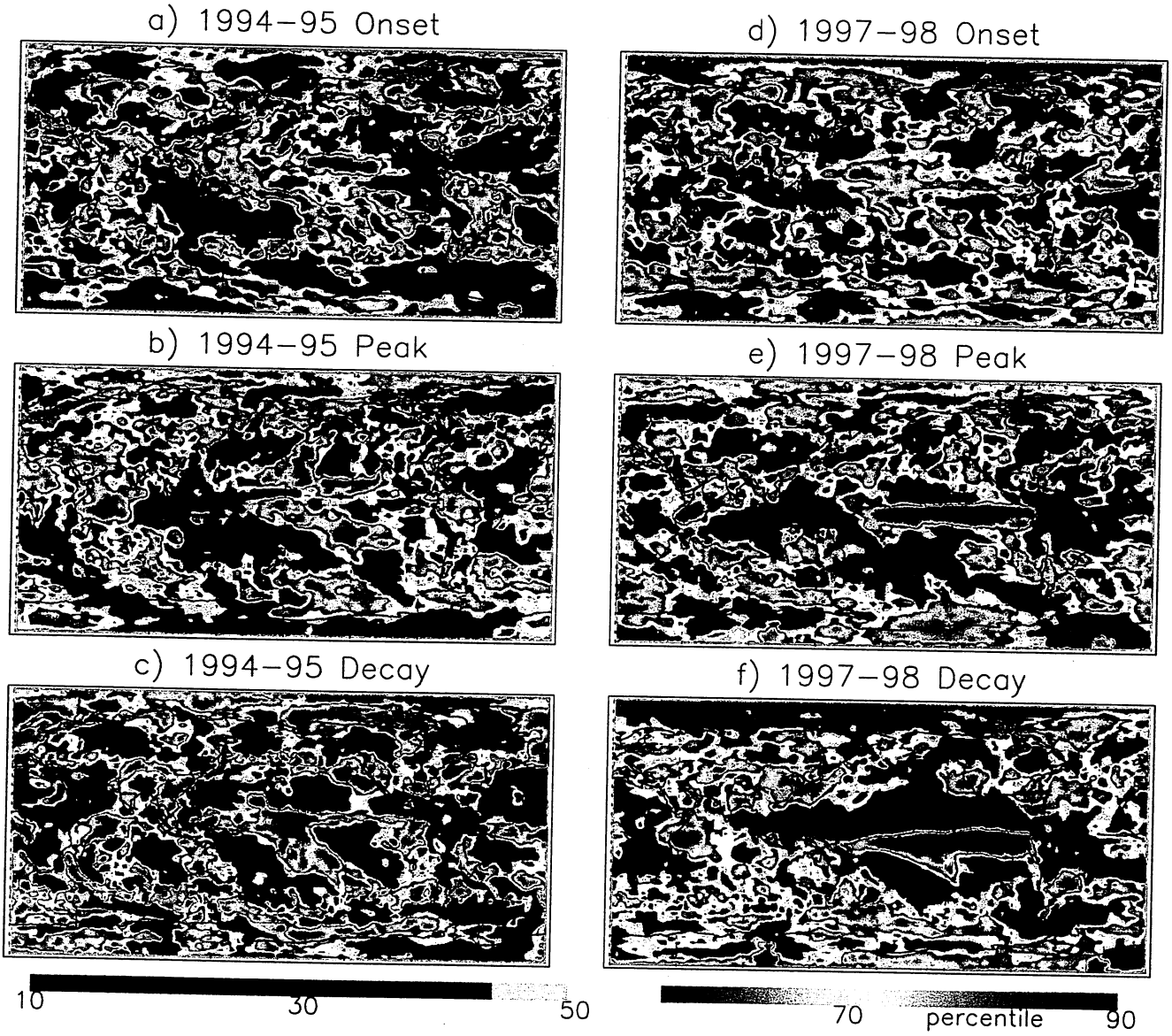
a) 1994–95 Onset
d) 1997–98 Onset
b) 1994–95 Peak
e) 1997–98 Peak
c) 1994–95 Decay
f) 1997–98 Decay
10
30
50
70
percentile
90

References

Aceituno, P., 1988: On the functioning of the Southern Oscillation in the South American sector. Part I: Surface climate. *Mon. Wea. Rev.*, 116, 505-525.

Adler, R. F., G. J. Huffman, A. Chang, R. Ferraro, P. Xie, J. Janowiak, B. Rudolf, U. Schneider, S. Curtis, D. Bolvin, A. Gruber, J. Susskind, and P. Arkin, 2002: The version 2 Global Precipitation Climatology Project (GPCP) monthly precipitation analysis (1979-present). *J. Hydromet.*, submitted.

Curtis, S. and R. Adler, 2000: ENSO indices based on patterns of satellite derived precipitation. *J. Climate*, 13, 2786-2793.

Curtis, S., R. Adler, G. Huffman, E. Nelkin, and D. Bolvin, 2001: Evolution of tropical and extratropical precipitation anomalies during the 1997-1999 ENSO cycle. *Int. J. Climatol.*, 21, 961-971.

Dai, A., and T. M. L. Wigley, 2000: Global patterns of ENSO-induced precipitation. *Geophys. Res. Lett.*, 27, 1283-1286.

Giannini, A., Y. Kushnir, and M. A. Cane, 2000: Interannual variability of Caribbean rainfall, ENSO, and the Atlantic Ocean. *J. Climate*, 13, 297-311.

Hastenrath, S., 1976: Variations in low-latitude circulation and extreme climatic events in the tropical Americas. *J. Atmos. Sci.*, 33, 202-215.

Hastenrath, S., 1984: Interannual variability and annual cycle: Mechanisms of circulation and climate in the tropical Atlantic sector. *Mon. Wea. Rev.*, 112, 1097-1107.

Huffman, G. J., R. F. Adler, P. Arkin, A. Chang, R. Ferraro, A. Gruber, J. Janowiak, A. McNab, B. Rudolf, U. Schneider, 1997: The Global Precipitation Climatology Project (GPCP) combined precipitation dataset.
Bull. Amer. Meteor. Soc., **78**, 5-20.

Kiladis, G. N., and H. Diaz, 1989: Global climatic anomalies associated with extremes in the Southern Oscillation. *J. Climate*, 2, 1069-1090.

Kousky, V. E., M. T. Kagano, and I. F. A. Cavalcanti, 1984: A review of the Southern Oscillation: Oceanic-atmospheric circulation changes and related rainfall anomalies. *Tellus*, 36A, 490-502.

Mason, S. J, and L. Goddard, 2001: Probabilistic precipitation anomalies associated with ENSO. *Bull. Amer. Meteor. Soc.*, 82, 619-638.

Rasmusson, E. M., and T. H. Carpenter, 1983: The relationship between eastern equatorial Pacific sea surface temperatures and rainfall over India and Sri Lanka. *Mon. Wea. Rev.*, 111, 517-528.

Ropelewski, C. F., and M. S. Halpert, 1986: North American precipitation and temperature patterns associated with the El Niño/Southern Oscillation (ENSO). *Mon. Wea. Rev.*, 114, 2352-2362.

Ropelewski, C. F., and M. S. Halpert, 1987: Global and regional scale precipitation patterns associated with the El Niño/Southern Oscillation. *Mon. Wea. Rev.*, 115, 1606-1626.

Ropelewski, C. F., and M. S. Halpert, 1996: Quantifying Southern Oscillation-precipitation relationships. *J. Climate*, 9, 1043-1059.

Sinclair, M. R., J. A. Renwick, and J. W. Kidson, 1997: Low-frequency variability of Southern Hemisphere sea level pressure and weather system activity. *Mon. Wea. Rev.*, 125, 2531-2543.

Smith, T. M., and C. F. Ropelewski, 1997: Quantifying Southern Oscillation-Precipitation relationships from an atmospheric GCM. *J. Climate*, 10, 2277-2284.

Susskind, J., P. Piraino, L. Rokke, L. Iredell, and A. Mehta, 1997: Characteristics of the TOVS pathfinder path A dataset. *Bull. Amer. Meteor. Soc.*, 78, 1449-1472.

Trenberth, K., E., 1997: The definition of El Niño. *Bull. Amer. Meteor. Soc.*, 78, 2771-2777.

Trenberth, K. E., and J. M. Caron, 2000: The Southern Oscillation revisited: Sea level pressures, surface temperatures, and precipitation. *J. Climate*, 13, 4358-4365.

Walker, G. T., and E. W. Bliss, 1932: World Weather V. *Mem. Roy. Meteor. Soc.*, 4, 53-84.

Xie, P. and P. Arkin, 1997: Global precipitation: a 17-year monthly analysis based on gauge observations, satellite estimates, and numerical model outputs. *Bull. Amer. Meteor. Soc.*, **78**, 2539-2558.

Xie, P. and P. Arkin, 1998: Global monthly precipitation estimates from satellite-observed outgoing longwave radiation. *J. Climate*, **11**, 137-164.

POPULAR SUMMARY

The Evolution of El Niño-Precipitation Relationships from Satellites and Gauges

by

Scott Curtis (JCET/UMBC)

And

Robert F. Adler (NASA/GSFC)

An El Niño is defined as warmer than normal waters in the eastern Pacific. El Niños last about a year and happen every 2 to 5 years. The warming of the ocean has an effect on the atmosphere leading to changes in global weather patterns. Many studies have examined how land regions become wetter or drier during El Niño. However, this study is one of the few that show El Niño-rainfall relationships over the entire globe. This is accomplished with satellite data that begins in 1979.

First, this study confirms that the effect of El Niño on rainfall is not random, but shows a global pattern resembling a horseshoe. The largest changes in precipitation occur in the tropics but fan out eastward and towards both the North and South Pole. Next the six strongest El Niños were examined. While the evolution of each El Niño was different, some precipitation changes were consistent among the six episodes. For example, overall the western U.S. is dry at the beginning of El Niño-years and wet at the end. Simple models were then used to characterize this sort of mutli-phase evolution for the globe. Areas were identified that either (1) started dry and ended wet (like the western U.S.), (2) started wet and ended dry, (3) started and ended dry, but were wet in the middle, or (4) started and ended wet, but were dry in the middle.

The objective of this study was to give scientists a global picture of precipitation changes during El Niños since 1979 and provide countries with new information so they can better prepare for El Niño from start to finish.